

Segmented Harmonic Loss: Handling Class-Imbalanced Multi-Label Clinical Data for Medical Coding with Large Language Models

Surjya Ray PhD, Pratik Mehta, Hongen Zhang MD, Ada Chaman,
Jian Wang PhD, Chung-Jen Ho PhD, Michael Chiou, Tashfeen Suleman
CloudMedx Inc.

Abstract

The precipitous rise and adoption of Large Language Models (LLMs) have shattered expectations with the fastest adoption rate of any consumer-facing technology in history. Healthcare, a field that traditionally uses NLP techniques, was bound to be affected by this meteoric rise. In this paper, we gauge the extent of the impact by evaluating the performance of LLMs for the task of medical coding on real-life noisy data. We conducted several experiments on MIMIC III and IV datasets with encoder-based LLMs, such as BERT. Furthermore, we developed Segmented Harmonic Loss, a new loss function to address the extreme class imbalance that we found to prevail in most medical data in a multi-label scenario by segmenting and decoupling co-occurring classes of the dataset with a new segmentation algorithm. We also devised a technique based on embedding similarity to tackle noisy data. Our experimental results show that when trained with the proposed loss, the LLMs achieve significant performance gains even on noisy long-tailed datasets, outperforming the F1-score of the state-of-the-art by over ten percentage points.

Keywords: Large Language Models, LLM, BERT, Transformer, NLP, Medical Coding, Multi-label, Extreme Class Imbalance, Long Tailed Distribution

1 Introduction

In the fall of 2019, Google incorporated BERT [9] in its US search engine for English language queries [29]. Two months later, they expanded the service to include over 70 languages worldwide for their non-English search engines [32]. BERT, a Large Language Model (LLM), was developed and introduced by Google less than a year prior [8]. This upgrade of Google’s search engine took place just two years after the introduction of BERT’s spiritual parent, the game-changing transformer architecture, by Vaswani et al. in 2017 [34]. Based on the encoder part of the original transformer architecture, BERT is excellent at Natural Language Understanding. This capability was essential to interpret and understand these unknown queries that the search engine faced, which accounts for 15% of its whopping 8.5 billion daily queries [29]. It was a gutsy move demonstrating its faith in the nascent technology, considering its ‘search and other’ revenues accounted for 58% of Alphabet’s total revenue [4].

Google was far from the only company aiding this meteoric rise and adoption of LLMs. ChatGPT, OpenAI’s transformer-based chatbot, garnered 100 million active users in January 2023, just two months after launch. It is the fastest adoption rate of any consumer-facing technology in history [18].

Healthcare, which has a long history of repurposing Natural Language Processing (NLP) techniques to interpret mammoth volumes of Electronic Medical Records (EMRs) and clinical notes, was bound to be affected by this LLM wave. The more pertinent question was what this adoption would look like and its extent.

Google was already investigating the possibilities of LLMs in healthcare with Med-PaLM [11], based on their Pathways Language Model, PaLM, a 540-billion parameter LLM [10]. At the same time, the World Health Organization called for caution against this precipitous adoption of LLMs for health-related purposes [2]. Without checks and balances, the decoder-based LLMs are prone to hallucinations, where a response may appear correct and relevant to those untrained in healthcare but is, in fact, erroneous. It may lead to “errors by healthcare workers, cause harm to patients, erode trust in AI, and thereby undermine or delay the potential long-term benefits and uses of such technologies around the world,” they worried [2].

To this end, we gauge the extent of the long-term usefulness of LLMs in healthcare, a field that requires stringent quality control due to strict regulations. It is a multifaceted initiative requiring experimentation on real-life healthcare data on various healthcare use cases. This paper reflects our initial exercises in that investigation. To make such a broad scope manageable, we picked the use case of medical coding of clinical notes for our initial assessment. Medical coding, which is the process of assigning standardized codes to a patient’s medical information, is a segment projected to reach \$38 billion by 2030. AI-aided medical coding is supposed to take at least \$5.71 Billion out of it [27]. This paper focuses on ICD codes (version 9 or ICD-9) [13], a system designed by WHO and used by healthcare professionals to classify and code diagnoses and procedures for claims processing. However, the methodology and implications that came out of this paper apply to all kinds of clinical coding.

As with all data-centric ML paradigms, we started with an in-depth analysis of various real-life datasets of unstructured EMRs, specifically MIMIC III and IV [21]. We quickly realized this data is highly imbalanced and heavily reliant on the note-taking practices of healthcare providers. These findings guided our research to realize the full potential of LLM for medical coding. Our key contributions can be summarized as follows: (1) We used a novel technique utilizing embedding similarity to preprocess and create labeled data from the two MIMIC datasets. Since the input of BERT is limited to 512 tokens, we could only include a fraction of the clinical notes that serve as inputs to our models. The method was instrumental in removing those ICD-9 codes that were absent in the chunk of input text, thereby reducing false positives in the training set. (2) We developed a new loss function, Segmented Harmonic Loss, to deal with the extreme class imbalance in a multi-label scenario after experimentation with existing methods, such as Focal Loss [24] or Class Balanced Loss [7], which failed to mitigate the problem effectively. We believe our study will provide practical guidelines for dealing with medical or other imbalanced data to unlock the full potential of data-centric ML approaches to harness the power of LLMs. (3) We achieved state-of-the-art MIMIC dataset benchmarks on medical coding, besting the previous results by more than ten percentage points, showcasing the potential of domain-specific LLMs in healthcare.

2 Data

Domain-specific finetuning of LLMs requires a considerable amount of data. In healthcare, Patient Health Information (PHI) is highly regulated by various laws to protect patient privacy, which varies from country to country. In the U.S., the Health Insurance Portability and Accountability Act of 1996 (HIPAA) [14] regulates how PHI may be released. The law specifies 18 types of identifiers, such as name, address, telephone numbers, medical record number, and other fields that must be deidentified before releasing any PHI. As a result, reliable and standardized open-source PHI and EMRs for research are hard to come by. The two data sources that meet the reliability and quality control required for research are MIMIC III and MIMIC IV datasets [21]. To date, these are the only large-scale, reliable, and freely accessible electronic health record datasets available [22] from the U.S. MIMIC III has around 60K records of PHI. MIMIC IV has around 300K, of which 200K are ICD-9 codes. The remaining 100K are the newer ICD-10 codes. In order to maximize our data, we created

an amalgamated dataset by extracting and combining the ICD-9 records from these two datasets. This process of preparing and preprocessing this dataset is described in the following subsections.

2.1 Data Format and Structure

Our data is comprised of two components: clinical notes (\mathbf{x}) and a list of corresponding codes assigned to the note (\mathbf{y}). Notes are unstructured text containing healthcare information like symptoms, diagnosis, medical services, and procedures noted by physicians and healthcare providers. Codes are the corresponding ICD-9 codes designated to the note by clinical coders. Together, they form one record of a note-code pair (\mathbf{x}, \mathbf{y}) . Denoting the k^{th} note-code pair as $(\mathbf{x}^k, \mathbf{y}^k)$, we can define our dataset as $\mathcal{D} = \{(\mathbf{x}^1, \mathbf{y}^1), (\mathbf{x}^2, \mathbf{y}^2), \dots, (\mathbf{x}^N, \mathbf{y}^N)\}$ where N is the number of training samples and $k \in \{1, 2, \dots, N\}$. For the scope of our problem, we consider \mathcal{C} codes or classes. Since we can have multiple ICD-9 codes (diagnoses, procedures and so on) for each note, the label for the k^{th} sample, \mathbf{y}^k , can be written as:

$$\mathbf{y}^k = [y_1^k, y_2^k, \dots, y_{\mathcal{C}}^k]^T \quad (1)$$

where:

y_i^k : label for the i^{th} class/code, & $y_i^k \in \{0, 1\}$,
 $i \in \{1, 2, \dots, \mathcal{C}\}$.

An example of note-code pair before vectorization is show in the Listing 1 and Table 1.

Listing 1 A truncated example of a note (\mathbf{x}) from the combined MIMIC dataset

```

symptomatic bradycardia permanent pacemaker placement chronic systolic
congestive heart failure coronary artery disease lastname 66794**] is
an — year old gentleman with a history of atrial fibrillation on
amiodarone and coumadin cad with 3vd seen on cardiac cath in [**2186**]
chf with ef of 20\% who initially presented to [**hospital1 **]
[**location (un) 620**] last night complaining of a slow heart beat.
per his wife at around midnight last night he came to bed complaining
that his heart was beating very slowly he felt weak and that he could
feel it in his chest. at that time he asked his wife to call 911 and
he was taken to [**hospital1 **] [**location (un) 620**] for further
evaluation. per his wife he did not complain of any chest pain
shortness of breath or nausea. also the family notes that he has been
having some falls/syncope at home including one event that he did not
remember in the past few weeks. . per ems report he was found to be
pale cool and diaphoretic on initial examination. ...

```

Table 1 Codes (\mathbf{y}) and their descriptions

Codes (y_i)	Description
42789	Other specified cardiac dysrhythmias
4263	Other left bundle branch block
2449	Acquired hypothyroidism
42822	Chronic systolic heart failure
41401	Coronary atherosclerosis of artery
3659	Glaucoma
4280	Congestive heart failure

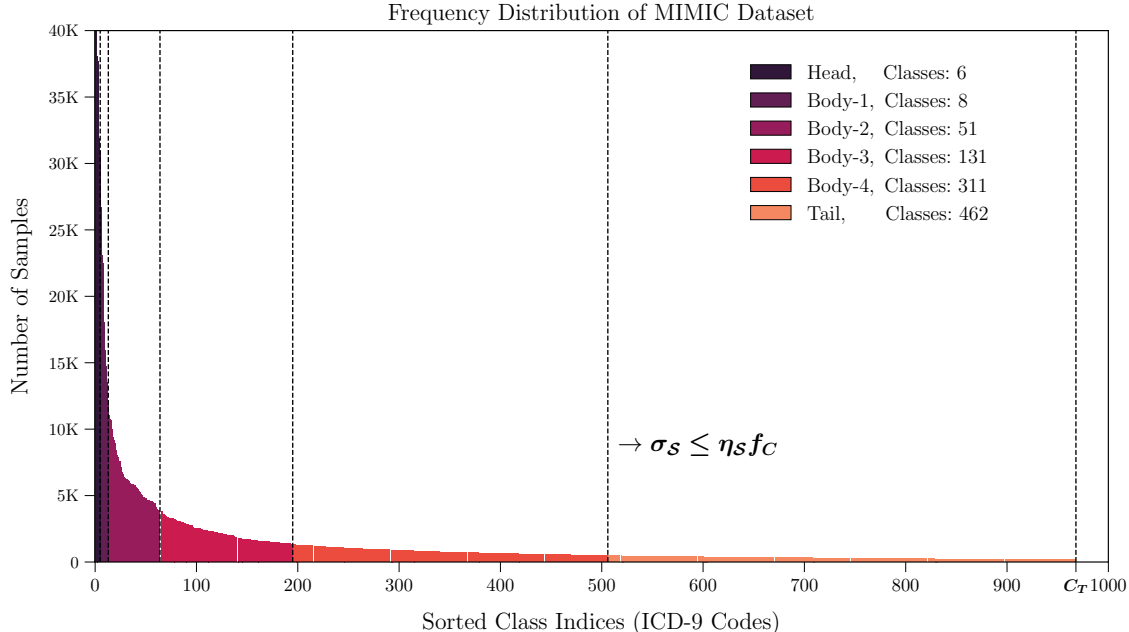


Fig. 1 The frequency distribution of the classes (ICD-9 codes) of the MIMIC dataset follows a long-tailed distribution. We use a recursive algorithm to segment the classes such that the standard deviation, σ_S , of the tail segment \mathcal{S} , does not exceed a fraction of the frequency, f_C , of the last class \mathcal{C} . The fraction, η_S , is a hyperparameter set to 0.5 in our experiments. Following this recursive algorithm, the classes of our dataset are divided into 6 segments with a head region, a tail region and four intermediate ‘body’ regions. **NOTE:** The frequency axis is shown upto 40K. The head classes actually goes upto around 80K.

2.2 Frequency Thresholding: Removal of Rare Codes

The combined dataset generated 261953 records or note-code pairs covering 9412 unique ICD-9 codes. The frequency distribution of the codes, sorted by frequency, is shown in Fig 1. We excluded codes with frequencies less than 200 as, at such low frequencies, they were not enough to train an LLM. As seen from Fig. 1, the frequency distribution of ICD-9 codes shows extreme class imbalance. It follows a long-tailed distribution. The ‘head’ part of the distribution contains only a few ICD-9 codes that occur frequently. The ‘tail’ end of the distribution contains a large number of codes whose frequency is several orders of magnitude lower than those codes in the ‘head’ section. In fact, the frequencies of the head classes are ≈ 700 times greater than those of the tail classes. In the first step of data preprocessing, we enforced a frequency threshold of 200 to the code list of every note-code pairs. This process removed 7924 unique codes from the code lists, leaving our dataset with 1488 codes with frequencies 200 and above.

2.3 Creation of the Input Notes (\mathbf{x})

The raw clinical notes were large, sometimes pages long, and were primarily free-form. With our medical professionals’ aid, we found that the diagnoses were primarily present in three essential sections:

- i. *Discharge Diagnosis*
- ii. *History of Present Illness*
- iii. *Past Medical History*

The last section was only relevant for diagnoses from past visits. In this paper, we focus only on current diagnoses. Hence, we created our inputs, \mathbf{x} , concentrating only on the first two sections, which are relevant for the current diagnoses. We also replaced medical abbreviations with corresponding texts, improving our results. In the provided example in 1, the abbreviation ‘CHF’ was replaced with

‘Congestive Heart Failure.’ If the text was longer than the input could accommodate, we truncated it to fit the input size of our LLM, which is limited to 512 tokens. If the text was shorter than the input size, we padded it to the maximum size of 512 tokens.

2.4 Similarity Thresholding: Removal of Invalid Codes

Because of the truncation step, many of the codes of label \mathbf{y} are not represented by the input note, \mathbf{x} , i.e., the diagnoses of these codes are not present in the truncated text for two reasons:

- i. The text of \mathbf{x} does not contain past medical history and hence does not contain codes from past visits.
- ii. Some codes from the current visit may not be represented in the text \mathbf{x} , as the truncation had removed the text containing the diagnoses.

We needed to remove these invalid codes from \mathbf{y} as these count as false positives. To achieve this, we used a technique of comparing embeddings using cosine similarities. To calculate the embeddings, we used the base model of clinicalBERT [37], which was trained on a large dataset with a large corpus of 1.2B words of diverse diseases created from EHRs from over 3 million patient records. We found it to be very efficient in incorporating bidirectional medical context and clinical meaning compared to similar encoder models. We passed each input note \mathbf{x} through ClinicalBERT and saved the last hidden state, \mathbf{h}_x , as shown in Fig 2. It is given by:

$$\mathbf{h}_x = [\mathbf{h}_x^1, \mathbf{h}_x^2, \dots, \mathbf{h}_x^{512}]^T \quad (2)$$

where \mathbf{h}_x^i is the i^{th} embedding out of the 512 embeddings in the final hidden state.

We use \mathbf{h}_x to create two sets of average embeddings, **Set A** and **Set B**. As shown in Fig 2, we divide the 512 embeddings of **Set A** into 64 groups, each containing eight embeddings. For each of these 64 groups, we calculate the mean embedding by averaging over the group. As seen from Fig 2, this produces a set of 64 mean embeddings given by:

$$\mathbf{h}_x^A = [\bar{\mathbf{h}}_1^A, \bar{\mathbf{h}}_2^A, \dots, \bar{\mathbf{h}}_{64}^A]^T \quad (3)$$

where $\bar{\mathbf{h}}_i^A$ is the mean embedding of the i^{th} group.

For **Set B**, we follow the same procedure as for **Set A**, except we divide the 512 embeddings into 32 groups of 16 embeddings. As for **Set A**, we compute the mean embeddings for these 32 groups giving:

$$\mathbf{h}_x^B = [\bar{\mathbf{h}}_1^B, \bar{\mathbf{h}}_2^B, \dots, \bar{\mathbf{h}}_{32}^B]^T \quad (4)$$

where $\bar{\mathbf{h}}_i^B$ is the mean embedding of the i^{th} group.

We treat each ICD-9 code present in \mathbf{y} separately. For each y_i in \mathbf{y} , we pass its official clinical text description (usually a few words) through ClinicalBERT. For example, if y_i corresponds to the code 42789 whose textual description is ‘Other specified cardiac dysrhythmias,’ we tokenize this text and pass it through the encoder. At the output, we get an equal number of embeddings as the number of input tokens. i.e., if the input text description had n tokens, the output hidden state, \mathbf{h}_{y_i} will have n embeddings. We create a mean embedding, $\bar{\mathbf{h}}_{y_i}$ by summing over all of these n embeddings.

To find out if y_i is present in the text in \mathbf{x} , we do the following:

1. Compute cosine similarities of $\bar{\mathbf{h}}_{y_i}$ with the 64 mean embeddings of \mathbf{h}_x^A in Equation 3.
2. Compute cosine similarities of $\bar{\mathbf{h}}_{y_i}$ with the 32 mean embeddings of \mathbf{h}_x^B in Equation 4.
3. Take the maximum similarity score of these two sets as the representative similarity score of y_i with \mathbf{x} .

The textual descriptions of y_i are usually a few words which results in a small number of input tokens \ll the 512 input tokens from \mathbf{x} . Slicing the 512 output embeddings of \mathbf{x} into chunks of 8 and 16 allows focusing on different parts of the input text. For smaller descriptions of y_i , usually, **Set A** performs better and for slightly larger descriptions of y_i , **Set B** performs better. We found that taking the maximum of the similarities of these two sets provided an optimal result with a similarity threshold of 0.55. We also tried taking cosine similarity of $\bar{\mathbf{h}}_{y_i}$ with the mean of 512 embeddings of

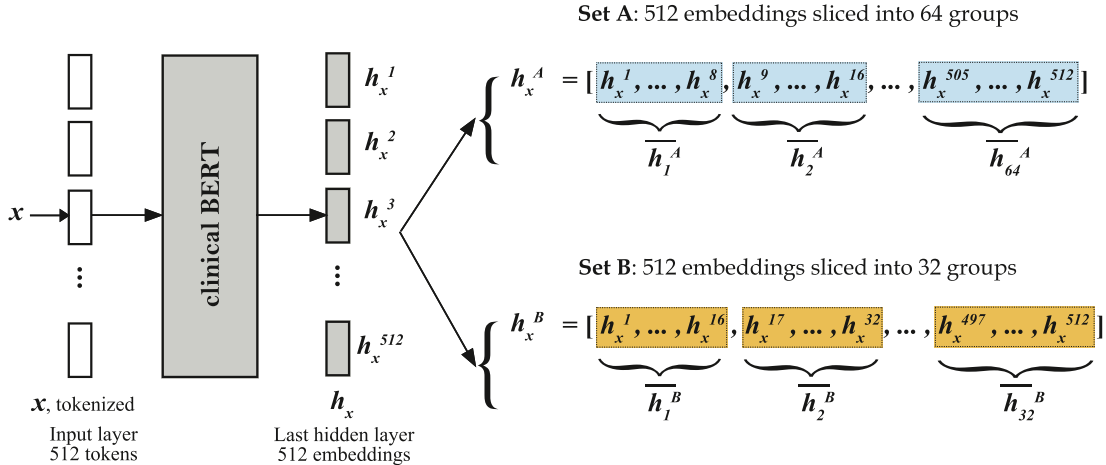


Fig. 2 The creation of two sets of mean embeddings using the output hidden state of ClinicalBERT

x . This does not perform well as averaging over so many embeddings dilutes the values of the relevant embeddings.

Table 2 shows cosine similarity of the codes of y associated with note x in Listing 1. The correct codes are chosen as those with a similarity above 0.55. On inspection of the note x , the selection of codes 42789, 42822, 41401 and 4280 are found to be correct.

Table 2 Codes (y_i) and their Similarity Scores with x

Codes (y_i)	Description	Similarity Score
42789	Other specified cardiac dysrhythmias	0.64
4263	Other left bundle branch block	0.50
2449	Acquired hypothyroidism	0.53
42822	Chronic systolic heart failure	0.72
41401	Coronary atherosclerosis of artery	0.66
3659	Glaucoma	0.44
4280	Congestive heart failure	0.72

After the step of similarity thresholding, codes that are not represented in the input text are removed from y . This alters the frequency distribution of the codes once more. Hence, we do frequency thresholding on the codes as before, removing any code that occurs less than 200 times in the dataset. After this exercise, we are left with 255736 records and a code set of 969 codes, which serves as our final dataset.

3 Segmented Training

We tried loss functions designed to mitigate class imbalance in multi-label scenarios, which we have included in our results in Section 4. With enough hyperparameter-tuning, these specialized loss functions improved the F_1 scores and other metrics over the standard Binary Cross Entropy (BCE) loss function, but the performance nevertheless degraded for the less-represented classes towards the tail region of the distribution. We surmise this is because a singular model could not fit the $1000\times$ order of discrepancy between the head and tail classes, especially with real-life noisy datasets. This led us to a different approach: fit separate models for different segments of the frequency distribution while decoupling co-occurring classes belonging to different segments using a new loss function. We formulate our problem mathematically in Subsection 3.1, describe our segmentation algorithm in Subsection 3.2, and discuss the loss function in Subsection 3.3.

3.1 Problem Formulation

As discussed in Subsection 2.1, our data are comprised of note-code pairs. We denote the k^{th} note-code pair as $(\mathbf{x}^k, \mathbf{y}^k)$, and our training dataset as $\mathcal{D} = \{(\mathbf{x}^1, \mathbf{y}^1), (\mathbf{x}^2, \mathbf{y}^2), \dots, (\mathbf{x}^N, \mathbf{y}^N)\}$ where N is the number of training samples and $k \in \{1, 2, \dots, N\}$. For the scope of our problem, we consider \mathcal{C} codes or classes. We sort and index these classes according to their frequencies as shown in Fig 1. This sorted list is denoted by \mathcal{F} where any index is a class id and the value at the index is the corresponding class frequency. This implies that two classes with indices l and m and frequencies f_l and f_m , will follow the relation $f_l \geq f_m$ if $l < m$ and $l, m \in \{1, 2, \dots, \mathcal{C}\}$. Since we can have multiple ICD-9 codes for each note, the label for the k^{th} sample, \mathbf{y}^k , can be written as:

$$\mathbf{y}^k = [y_1^k, y_2^k, \dots, y_{\mathcal{C}}^k]^T \quad (5)$$

where:

y_i^k : label for the i^{th} class/code, & $y_i^k \in \{0, 1\}$,
 $i \in \{1, 2, \dots, \mathcal{C}\}$.

This is a multi-label classification problem, i.e. the occurrence of $y_i^k = 1$ and $y_j^k = 1$, where $i \neq j$ and $i, j \in \{1, 2, \dots, \mathcal{C}\}$, are not necessarily mutually exclusive. Thus, given a clinical note \mathbf{x}^k , our objective is to predict the associated classes(ICD-9 codes), i.e. \mathbf{y}^k .

3.2 Segmentation Algorithm

The Segmentation Algorithm divides the list \mathcal{F} into \mathcal{S} segments. The r^{th} segment, \mathcal{F}_r , has c_r classes such that $\sum_{r=1}^{\mathcal{S}} c_r = \mathcal{C}$. The algorithm starts by creating the tail segment, $\mathcal{F}_{\mathcal{S}}$, by grouping the last $c_{\mathcal{S}}$ classes of the tail such that there is a relatively small variation between their class frequencies. The amount of tolerable variation is controlled by a hyperparameter $\eta_{\mathcal{S}}$ such that:

$$\sigma_{\mathcal{S}} \leq \eta_{\mathcal{S}} f_{\mathcal{C}}. \quad (6)$$

where:

$f_{\mathcal{C}}$: the frequency of the last class \mathcal{C} .
 $\sigma_{\mathcal{S}}$: the standard deviation of the class frequencies of segment $\mathcal{F}_{\mathcal{S}}$.
 $\eta_{\mathcal{S}}$: a hyperparameter in $(0, 1]$ which determines the tolerable variance, $\sigma_{\mathcal{S}}^2$, between the class frequencies of segment $\mathcal{F}_{\mathcal{S}}$.

For example, if $\eta_{\mathcal{S}}$ is set to 0.5, $\sigma_{\mathcal{S}}$ can be at most half of the last class frequency, $f_{\mathcal{C}}$. Thus, the choice of $\eta_{\mathcal{S}}$ shall control the amount of tolerable variation between frequencies in a segment and will in turn control i) the number of segments, \mathcal{S} , and ii) the size of the segments i.e. the number of classes in these respective segments.

Once segment $\mathcal{F}_{\mathcal{S}}$ has been generated, we are left with $\mathcal{C}' = \mathcal{C} - c_{\mathcal{S}}$ classes which approximate another long-tailed distribution. We recursively create more segments from the tail end, until there are no more classes left. The pseudo-code of the segmentation algorithm is shown in Algorithm 1. The procedure SEGMENTF recursively segments the list \mathcal{F} from the tail end such that Equation 6 is satisfied. Inside this procedure, another procedure, SEGMENTTAIL, is used to create one segment at a time from the tail end. This procedure returns the index of the first class to be included in the segment being computed. It is denoted by i_{start} in the pseudocode. The procedure SEGMENTTAIL maybe efficiently implemented using Binary Search and its pseudocode is presented in Appendix A. Following this algorithm, our dataset is divided into six segments (\mathcal{F}_1 through \mathcal{F}_6) as shown by the dotted vertical lines in Fig 1 with $\mathcal{S} = 6$.

Once \mathcal{F} is segmented into \mathcal{S} segments, the k^{th} sample $\{\mathbf{x}^k, \mathbf{y}^k\}$, presented in Equation 5 yields \mathcal{S} labels $\mathbf{y}^{k,r}$, one for each segment, where the second superscript indicates the segment number, i.e.,

Algorithm 1 Partition list \mathcal{F} into segments

```

1: //segments: List of segments.
2: segments  $\leftarrow$  []
3: //F: index-sorted list of class frequencies
4:
5: procedure SEGMENTF( $\mathcal{F}$ ,  $\eta_S$ , segments)
6:    $n \leftarrow \text{len}(\mathcal{F})$ 
7:   // If list  $\mathcal{F}$  is not empty, create a segment  $\mathcal{F}_{curr}$  from the tail end
8:   if  $n > 0$  then
9:     // Get index of the last class of  $\mathcal{F}_{curr}$ 
10:     $i_{end} \leftarrow n$ 
11:    // Get index of the first class of  $\mathcal{F}_{curr}$ 
12:     $i_{start} \leftarrow \text{SEGMENTTAIL}(\mathcal{F}, \eta_S)$ 
13:    // Create the current segment  $[i_{start}, i_{end}]$ 
14:     $\mathcal{F}_{curr} \leftarrow [i_{start}, i_{end}]$ 
15:    // Add the current segment to list segments.
16:    segments.append( $\mathcal{F}_{curr}$ )
17:    // Update  $\mathcal{F}$  by discarding segment  $\mathcal{F}_{curr}$ 
18:     $\mathcal{F} \leftarrow \mathcal{F}[1 : i_{start}]$ 
19:    // Recursively call the procedure.
20:    SEGMENTF( $\mathcal{F}$ ,  $\eta_S$ , segments)
21:   end if
22:   return
23: end procedure

```

$r \in \{1, 2, \dots, \mathcal{S}\}$. Thus, the label for the k^{th} note-code pair $(\mathbf{x}^k, \mathbf{y}^{k,r})$ of segment \mathcal{F}_r is:

$$\mathbf{y}^{k,r} = [y_{\rho+1}^{k,r}, y_{\rho+2}^{k,r}, \dots, y_{\rho+c_r}^{k,r}]^T \quad (7)$$

where:

- c_r : number of classes in segment \mathcal{F}_r ,
- ρ : total number of classes in the first $r - 1$ segments = $\sum_{p=1}^{r-1} c_p$,
- $y_i^{k,r}$: label for the i^{th} class/code & $y_i^{k,r} \in \{0, 1\}$,
- $i \in \{\rho + 1, \rho + 2, \dots, \rho + c_r\}$.

Although we derive the segmentation algorithm using the example of a long-tailed imbalanced distribution, the algorithm works for all kinds of imbalanced distributions as long as we order the classes according to their frequencies.

We train each segment model on all N training samples. This helps in decoupling co-occurring classes (ICD-9 codes). Consider two co-occurring classes i and j for the k^{th} label, \mathbf{y}^k . This implies $y_i^k = 1$ and $y_j^k = 1$, where $i \neq j$ and $i, j \in \{1, 2, \dots, \mathcal{C}\}$. Let's assume $i \in \mathcal{F}_r$ and $j \notin \mathcal{F}_r$. When training for the segment \mathcal{F}_r , the sample $\mathbf{y}^{k,r}$, derived from \mathbf{y}^k , shall ignore the class j , thereby teaching the model of segment \mathcal{F}_r to discriminate against the j^{th} class. This decouples the class j from segment \mathcal{F}_r .

If \mathbf{x}^k does not represent any classes for segment \mathcal{F}_r , its label, $\mathbf{y}^{k,r}$, will be a zero vector i.e. $\mathbf{y}^{k,r} = [0, 0, \dots, 0]^T$. These serve as negative samples for segment \mathcal{F}_r . The number of negative samples contributed by segments other than \mathcal{F}_r may be orders of magnitude more than positive samples coming from \mathcal{F}_r . Unless suitably down-weighted, the loss contributions from these negative samples will overwhelm the training loss while using a traditional loss function such as BCE. This is why we need a new loss function to modulate the loss contributions from negative samples.

3.3 Segmented Harmonic Loss

We use segment \mathcal{F}_r for the formulation of the new loss function. After segmentation, each segment will contain classes with tolerable variance between their frequencies. However, the positive examples of any class from \mathcal{F}_r (*positive segment*) may be orders of magnitude less than negative samples contributed by the classes present in the remaining $\mathcal{S} - 1$ segments (*negative segments*). At the same time, these negative examples are necessary for the learning process of \mathcal{F}_r 's model to discriminate between positive and negative samples.

Segmented Harmonic (SH) loss allows us to train models of different segments on the entire dataset of N samples by achieving the following goals of our loss function:

Goal 1: Balance the loss contributions from the negative samples during training by dynamically weighing their losses.

Goal 2: Penalize classification errors for negative samples by dynamically increasing the corresponding loss.

Goal 3: Penalize classification errors for harder-to-classify samples by dynamically increasing the corresponding loss.

Since we are dealing with multi-label classification, a Binary Cross Entropy (BCE) loss provides a good starting point for the formulation. For simplicity, we shall denote the k^{th} sample, so far denoted as $(\mathbf{x}^k, \mathbf{y}^{k,r})$, as $(\mathbf{x}, \mathbf{y}^r)$ removing the superscript k indicating the sample number. Let \mathbf{p}^r be the prediction of \mathbf{y}^r and \mathbf{y} be the original label before segmentation. BCE Loss for a single class in \mathcal{F}_r is given by:

$$BCE(p^r, y^r) = \begin{cases} -\log(p^r) & \text{if } y^r = 1 \\ -\log(1 - p^r) & \text{otherwise} \end{cases} \quad (8)$$

where $p^r \in [0, 1]$ is the prediction probability for the label $y^r = 1$ in the single-class case. For notational convenience, we define q^r as:

$$q^r = \begin{cases} p^r & \text{if } y^r = 1 \\ 1 - p^r & \text{otherwise} \end{cases} \quad (9)$$

Using Equation 9, we rewrite BCE as:

$$BCE(p^r, y^r) = BCE(q^r) = -\log(q^r) \quad (10)$$

Considering the multi-label scenario of segment \mathcal{F}_r , we can write the Cross Entropy (CE) loss using Equation 10 as:

$$CE(\mathbf{q}^r) = -\sum_{i=1}^{c_r} \log(q_i^r) \quad (11)$$

where:

- c_r : number of classes in segment \mathcal{F}_r ,
- $\mathbf{q}^r = [q_{\rho+1}^r, q_{\rho+2}^r, \dots, q_{\rho+c_r}^r]^T$,
- ρ : total number of classes in the first $r - 1$ segments = $\sum_{p=1}^{r-1} c_p$,

To meet **Goal 1**, we need to include a modulating term in Equation 11 that will temper the contributions of the samples from negative segments which are far more in number than the positive examples. We start by calculating the approximate rates of occurrences of samples from the i^{th} negative segment \mathcal{F}_i , w.r.t the positive samples from \mathcal{F}_r . Let \mathbb{N}_i be the number of positive samples from segment \mathcal{F}_i . We define the approximate rate of occurrence of samples from \mathcal{F}_i w.r.t \mathcal{F}_r as:

$$\beta^{(i,r)} = \frac{\mathbb{N}_i}{\mathbb{N}_r} \quad (12)$$

If the label \mathbf{y}^r is a negative sample i.e. a zero vector, its original label \mathbf{y} must contribute to at least one segment other than \mathcal{F}_r . For example, if \mathbf{y} contains two positive classes belonging to segment \mathcal{F}_l , and one to segment \mathcal{F}_m , we can approximate the mean rate for observing this particular negative sample \mathbf{y}^r as:

$$\beta^{SH} = \mathbf{mean}(\beta^{(l,r)}, \beta^{(l,r)}, \beta^{(m,r)}) = \mathbf{mean}(2\beta^{(l,r)}, \beta^{(m,r)}) \quad (13)$$

Different aggregate measures may be used to implement the $\mathbf{mean}()$ of Equation 13. Since we are aggregating rates, it is best implemented using harmonic mean. Thus, we can rewrite Equation 13 as:

$$\beta^{SH} = \frac{2 + 1}{\frac{2}{\beta^{(l,r)}} + \frac{1}{\beta^{(m,r)}}} \quad (14)$$

In general, if the original label \mathbf{y} contain n_i positive classes belonging to segment \mathcal{F}_i where $i \in \{1, 2, \dots, S\}$ and $i \neq r$, the approximate the mean rate for observing the negative sample \mathbf{y}^r is given by:

$$\beta_r^{SH} = \frac{\sum_{i=1}^S n_i}{\sum_{i=1}^S \frac{n_i}{\beta^{(i,r)}}} \quad (15)$$

In Equation 15, since \mathbf{y}^r is a negative sample originating from \mathbf{y} , there are no positive classes in \mathbf{y}^r , i.e. $n_r = 0$. Note that β_r^{SH} can never be undefined which is discussed in Appendix B. The Segmented Harmonic (SH) loss is given by the following equation by incorporating a modulating factor of $\frac{1}{\beta_r^{SH}}$:

$$SH(\mathbf{q}^r) = -\frac{1}{\beta_r^{SH}} \sum_{i=1}^{c_r} \log(q_i^r) \quad (16)$$

Since β_r^{SH} is the mean rate for observing the negative sample \mathbf{y}^r , a modulating factor inversely proportional to its occurrence rate will balance the contribution of this negative sample to the training loss, hence satisfying **Goal 1**. We have found that introducing β_r^{SH} in positive examples improves stability of the loss function. It is calculated in the same way as the negative examples.

To meet the requirements of **Goal 2** and **3** we take inspiration from Focal Loss [24] and incorporate a term $(1 - q^r)^\gamma$ in Equation 16. Thus we obtain SH Focal Loss as:

$$SH_{Focal}(\mathbf{q}^r) = -\frac{1}{\beta_r^{SH}} \sum_{i=1}^{c_r} (1 - q^r)^\gamma \log(q_i^r) \quad (17)$$

The focusing parameter $\gamma \geq 0$ from Focal Loss [24] penalizes the loss function for making mistakes on ‘‘hard-to-classify’’ instances. In our experiments, we tried $\gamma \in \{1.5, 2.0, 2.5\}$ and found 2, as suggested by the authors to work best. Details of Focal loss can be found in the paper [24].

4 Experiments

We describe our experimental setup in Subsection 4.1, its challenges and workarounds in Subsection 4.2, and model selection in Subsection 4.3.

4.1 Experimental Setup

Traditionally, the new era of machine learning has been widely successful because of GPU computing. From safety-critical applications such as autonomous driving, [5] to drug discovery [31], GPU computing has been an essential ingredient, and much of this market (over 70%) is dominated by NVIDIA [6]. Almost all, if not all, LLMs depend on NVIDIA’s CUDA-enabled GPU architecture. For initial experimental setup, coding, and debugging, we used a machine with a single NVIDIA A10G GPU with 24 GB of GPU Memory. For training, we used a machine with four NVIDIA A10G GPUs, each GPU having a dedicated memory of 16 GB.

4.2 Setup Challenges

Initially, we faced several implementation / resource-related challenges well-known to the machine-learning community, which mirrored the GPU resource-related problems faced by Deep Learning in its early days. This problem is exacerbated in LLMs because of their sheer size. While the larger Deep Neural Networks had an average of 50 million parameters, even the simplest LLM, such as the base clinicalBERT, has a parameter count of 110 million. GPT-J has 6 billion parameters, while the Llama-2 models start at 7 billion and go up to 70 billion parameters. When trained without optimization, GPT-J requires a minimum of 90 GB to load. To combat this resource-hungry aspect of LLMs, an entire sub-discipline of machine learning dedicated to optimizing GPU resources for the training and inference of LLMs has emerged [15]. The frameworks, libraries, and techniques we used to run these massive models are:

- i. **LoRA**: Low-Rank Adaptation, or LoRA [17], is a framework that significantly reduces the trainable parameters by freezing the pretrained model weights and injecting trainable rank decomposition matrices into the LLM architecture [17]. LoRA, known to reduce the number of trainable parameters by as much as 10,000 times and the GPU memory requirement by three times, was quite effective in running large LLMs such as Llama-2 on our smaller machines.
- ii. **Mixed-precision training**: This refers to the use of lower-precision formats than *float32* such as *float16* in an LLM during training, making it faster and use less memory while ensuring that compared to full precision training no task-specific accuracy is lost [1].
- iii. **Quantization**: It is the process of running inference by representing the weights and activations with lower precision data types, reducing memory footprint, such as replacing *float32* with *float16*, making it possible to achieve as much as 2x reduction in memory usage [20].
- iv. **xTuring**: xTuring [3] is an open-source library that simplifies the process of building, controlling, and tuning LLMs with a simple interface for personalizing the models to suit the application requirements. This library includes many of the above optimizations, such as LoRA, and was instrumental in getting Llama-2 and GPT-J running.

4.3 LLM Base Model Selection

After initial experimentation on various architectures, we settled on a BERT encoder architecture for our base model over generative models such as GPT-J [36] or Llama-2 [12]. A heavily quantized *int4* version of GPT-J further optimized by LoRA (training only 1% of its trainable parameters) fitted in our training machine’s 16 GB GPU RAM. Although it did not take significant time to run (3 hours), the model did not converge and produced abysmal results. Furthermore, being a generative model, the ICD-9 codes needed to be introduced in the vocabulary for the tuned model to predict the codes given an input note.

We also performed experiments with Llama-2 (7B) using 8-bit quantization and optimized by LoRA (training < 0.5% of its trainable parameters). However, the time required to complete one epoch on the single GPU machine was ten days and 2.5 days on the training machine. It was prohibitively expensive, and we discontinued the experiments after two days on the single GPU server.

The BERT architecture fitted in our memory without mixed precision, but we used mixed precision for faster convergence. Its bidirectional encoding was ideal for classification purposes, and unlike generative models, it did not require any addition to vocabulary as it treated the codes as classes. Since we needed a deeper understanding of medical jargon and vocabulary, we settled on ClinicalBERT, a model identical in size and architecture to BERT but was imbued with medical vocabulary. We also used it for data preprocessing. ClinicalBERT was initialized from BERT and trained on a large dataset of EHRs from over 3 million patient records. It performed much better (more than ten percentage points on micro F1 score) than Microsoft’s PubMedBERT [16], which was pretrained from scratch using abstracts from PubMed [30] as well as full-text articles from PubMedCentral. The poor performance of PubMedBERT on the MIMIC dataset exemplifies the necessity of training base models on real-life data, which in our case are free-form handwritten notes and not fully formed text obtained from paper abstracts.

5 Results

We trained our model for 150,000 steps or 8 hours, each step taking approximately 0.19 seconds. Using stratified sampling, we split the dataset into training, validation and test datasets in the ratio of 94 : 3 : 3. Stratified sampling ensured that our split was unbiased, and captured key population characteristics i.e. included all classes including minority classes as in the training set.

Table 3 Micro F1 scores for the total MIMIC Dataset and its different segments

Methods	Total	Head	Body 1	Body 2	Body 3	Body 4	Tail
BCE-BERT	69.87	70.74	68.61	65.40	58.96	54.31	46.03
Focal-BERT	71.42	72.97	73.83	68.93	63.00	60.23	42.50
CB-Focal-BERT	69.91	71.01	71.93	67.93	61.07	58.42	51.87
SH-Focal-BERT	71.28	72.73	77.01	71.31	64.22	61.63	59.81

For all experiments, we used AdamW optimizer [26] with default settings except for the learning rate, which we initialized to 0.0005. We used Binary Cross Entropy (BCE) as the baseline loss function. Since our data is highly imbalanced, we did not try resampling techniques [33] because they are not effective for multi-label scenarios in NLP. Instead, we tried various loss functions such as Focal Loss [24] and Class-Balanced Loss (CB) [7], which are designed to mitigate class imbalance in multi-label scenarios. For Focal Loss, the focusing hyperparameter γ that worked best for us is 2. For Class-Balanced Loss, we set the hyperparameter β to 0.99. The β_r^{SH} for Segmented Harmonic Loss is calculated based on the dataset and the hyperparameter η_S , which we set to a value of 0.5.

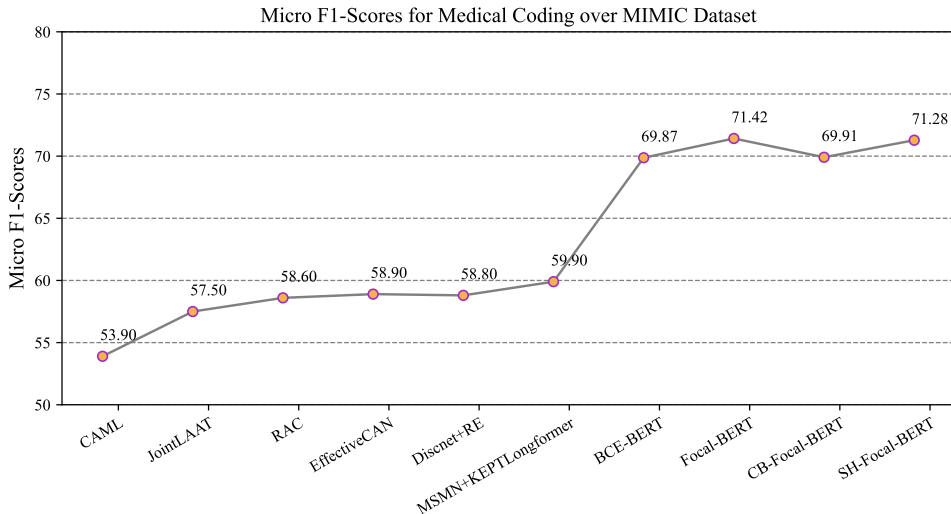


Fig. 3 Micro F1 score comparisons with well known approaches: CAML [28], JointLAAT [35], RAC[23], EffectiveCAN[25], Discnet+RE[39], MSMN+LongFormer[38].

For performance metrics, we used *segment-wise micro F1 score*. Since macro F1 scores treat all classes equally regardless of their support values, a simple average may be a misleading performance metric for imbalanced distributions. Micro F1 score, which gives equal weights to each sample regardless of its class, is also not particularly suitable as a majority class can dominate its value. Instead, we segmented the imbalanced distribution using the equation 6. The hyperparameter η_S 's value segmented the dataset into six segments with comparable variance. For each segment, we calculated a micro F1 score or *segment-wise micro F1 score*.

Table 3 shows the performance of different losses with clinicalBERT as the base. Segmented Harmonic Focal Loss (abbreviated as SH-Focal-BERT) performs much more evenly than Focal Loss (Focal-BERT), whose micro F1 scores degrade towards the tail end. The same happens for Class-Balanced Focal loss (CB-Focal-BERT), though it fares better towards the tail region. Segmented Harmonic Focal Loss performs the best through all segments, though its total micro F1 score is marginally less than the Focal-BERT configuration.

In general, the effect of LLMs over other approaches is evident from Figure 3. There is a ten percentage point jump from the approach in [38]. Although most of these approaches worked with only the MIMIC III dataset and did not enhance their dataset with records from MIMIC IV, the performance gain is not solely due to the larger dataset. Our initial experiments with only the MIMIC III dataset showed a seven percentage point gain over previous approaches such as in [38].

6 Conclusion & Future Work

The fact that LLMs would outperform previous architectures by as much as ten percentage points was not surprising to us. Vaswani et al.’s transformer architecture has proven to be superior over Recurrent Neural Networks over and over again and has rewritten the book in NLP. With Harmonic Loss developed to tackle multi-label extreme imbalance, the results improved even more for the minority classes. It would not be surprising either if a different approach to cleaning and dealing with class imbalance yields even better results.

However, our experiments, particularly our failure to tackle the extra-large models, reveal something more telling: domain-specific training of LLMs can be prohibitively expensive until the hardware catches up with the rapid progress in R&D. The healthcare sector has always been wary of using open-source software. LLMs trained on a big chunk of the internet, books, and other text sources are subject to litigations [19], and healthcare companies are wary of it. It hinders the adoption of this marvel of technology.

Another key takeaway is a bigger LLM is not essential for good results. A highly regulated domain like healthcare requires quality control and replicability of results. In our future work, those are the aspects we would like to explore: how do we build sufficiently large LLMs from scratch in-house, one that protects patients’ privacy, have stringent quality control measures, and replicability of results? We believe that would unlock the full potential of LLMs in healthcare.

Appendix A Pseudocode for procedure SEGMENTTAIL

A Binary-Search-based implementation of the procedure SEGMENTTAIL is given below. STD is any procedure to compute standard deviation of a list.

Appendix B Differentiability of Segmented Harmonic Loss

For $\mathbf{q}^r \in (0, 1)$, Segmented Harmonic Loss as defined in equation 17 is differentiable. Any negative sample \mathbf{y}^r belonging to \mathcal{F}_r must contribute at least one positive sample belonging to other segments. This will result in a positive harmonic mean β_r^{SH} . Thus, the modulating term $\frac{1}{\beta_r^{SH}}$ is always positive and can never be undefined. The remaining factor in equation 17 is essentially BCE and Focal Loss whose derivatives and differentiability has been proven in [24].

References

- [1] Train with mixed precision. <https://docs.nvidia.com/deeplearning/performance/mixed-precision-training/index.html>, Feb 2023.
- [2] WHO calls for safe and ethical ai for health. <https://www.who.int/news/item/16-05-2023-who-calls-for-safe-and-ethical-ai-for-health>, May 2023.
- [3] xTuring - build and control your own LLMs. <https://xturing.stochastic.ai/>, 2023.

Algorithm 2 Return the starting index of the tail segment \mathcal{F}_S

```
1: procedure SEGMENTTAIL( $\mathcal{F}, \eta_S$ )
2:   //  $\mathcal{F}$ : index-sorted list of class frequencies
3:    $n \leftarrow \text{len}(\mathcal{F})$ 
4:   // Initialize the left pointer for Binary Search
5:    $left \leftarrow 0$ 
6:   // Initialize the right pointer for Binary Search
7:    $right \leftarrow (n - 1)$ 
8:   // Compute the allowed standard deviation using  $\eta_S$  and the last frequency of  $\mathcal{F}$ 
9:    $\sigma_{allowed} \leftarrow \eta_S \times \mathcal{F}[n - 1]$ 
10:  // Find the starting index of the tail segment  $\mathcal{F}_S$ 
11:  while  $left < right$  do
12:    // Get the middle index
13:     $mid \leftarrow (left + right)/2$ 
14:    // Get the standard deviation of  $\mathcal{F}[mid :]$ 
15:     $\sigma_{mid} \leftarrow \text{STD}(\mathcal{F}[mid :])$ 
16:    if  $\sigma_{mid} > \sigma_{allowed}$  then
17:       $left = mid + 1$ 
18:    else if  $\sigma_{mid} < \sigma_{allowed}$  then
19:       $right = mid$ 
20:    end if
21:  end while
22: return  $left$ 
23: end procedure
```

- [4] Tiago Bianchi. Alphabet: Global annual revenue by segment 2022. <https://www.statista.com/statistics/633651/alphabet-annual-global-revenue-by-segment/>, Feb 2023.
- [5] Mariusz Bojarski, Davide Testa, Daniel Dworakowski, Bernhard Firner, Beat Flepp, Prasoon Goyal, Larry Jackel, Mathew Monfort, Urs Muller, Jiakai Zhang, Xin Zhang, Jake Zhao, and Karol Zieba. End to end learning for self-driving cars. 04 2016.
- [6] Don Clark. How nvidia built a competitive moat around a.i. chips. <https://www.nytimes.com/2023/08/21/technology/nvidia-ai-chips-gpu.html>, Aug 2023.
- [7] Yin Cui, Menglin Jia, Tsung-Yi Lin, Yang Song, and Serge Belongie. Class-balanced loss based on effective number of samples. In *2019 IEEE/CVF Conference on Computer Vision and Pattern Recognition (CVPR)*, pages 9260–9269, 2019.
- [8] Jacob Devlin and Ming-Wei Chang. Open sourcing bert: State-of-the-art pre-training for natural language processing. <https://ai.googleblog.com/2018/11/open-sourcing-bert-state-of-art-pre.html>, Nov 2018.
- [9] Jacob Devlin, Ming-Wei Chang, Kenton Lee, and Kristina Toutanova. BERT: pre-training of deep bidirectional transformers for language understanding. In Jill Burstein, Christy Doran, and Thamar Solorio, editors, *Proceedings of the 2019 Conference of the North American Chapter of the Association for Computational Linguistics: Human Language Technologies, NAACL-HLT 2019, Minneapolis, MN, USA, June 2-7, 2019, Volume 1 (Long and Short Papers)*, pages 4171–4186. Association for Computational Linguistics, 2019.
- [10] Chowdhery et al. Palm: Scaling language modeling with pathways. *ArXiv*, abs/2204.02311, 2022.

- [11] Singhal et al. Large language models encode clinical knowledge. *Nature*, 620(7972):172–180, 2023.
- [12] Touvron et al. Llama 2: Open foundation and fine-tuned chat models, 2023.
- [13] Centers for Disease Control and Prevention. ICD - ICD-9-CM - international classification of diseases, ninth revision, clinical modification. <https://www.cdc.gov/nchs/icd/icd9cm.htm>, Nov 2021.
- [14] Centers for Disease Control and Prevention. Health insurance portability and accountability act of 1996 (hipaa). <https://www.cdc.gov/phlp/publications/topic/hipaa.html>, Jun 2022.
- [15] Yanjie Gao, Yu Liu, Hongyu Zhang, Zhengxian Li, Yonghao Zhu, Haoxiang Lin, and Mao Yang. Estimating gpu memory consumption of deep learning models. pages 1342–1352, 11 2020.
- [16] Yu Gu, Robert Tinn, Hao Cheng, Michael Lucas, Naoto Usuyama, Xiaodong Liu, Tristan Naumann, Jianfeng Gao, and Hoifung Poon. Domain-specific language model pretraining for biomedical natural language processing, 2020.
- [17] Edward J. Hu, Yelong Shen, Phillip Wallis, Zeyuan Allen-Zhu, Yuanzhi Li, Shean Wang, Lu Wang, and Weizhu Chen. Lora: Low-rank adaptation of large language models, 2021.
- [18] Krystal Hu. ChatGPT sets record for fastest-growing user base - analyst note. <https://www.reuters.com/technology/chatgpt-sets-record-fastest-growing-user-base-analyst-note-2023-02-01/>, Feb 2023.
- [19] Hillel Italie. “game of thrones” creator and other authors sue chatgpt-maker openai for copyright infringement. <https://apnews.com/article/openai-lawsuit-authors-grisham-george-rr-martin-37f9073ab67ab25b7e6b2975b2a63bfe>, Sep 2023.
- [20] Benoit Jacob, Skirmantas Kligys, Bo Chen, Menglong Zhu, Matthew Tang, Andrew Howard, Hartwig Adam, and Dmitry Kalenichenko. Quantization and training of neural networks for efficient integer-arithmetic-only inference. In *2018 IEEE/CVF Conference on Computer Vision and Pattern Recognition*, pages 2704–2713, 2018.
- [21] Alistair Johnson, Lucas Bulgarelli, Tom Pollard, Steven Horng, Leo Anthony Celi, and Roger Mark. MIMIC-IV. <https://physionet.org/content/mimiciv/1.0/>, 2021.
- [22] Alistair Johnson, Lucas Bulgarelli, Lu Shen, Alvin Gayles, Ayad Shammout, Steven Horng, Tom Pollard, Sicheng Hao, Benjamin Moody, Brian Gow, Li-wei Lehman, Leo Celi, and Roger Mark. MIMIC-IV, a freely accessible electronic health record dataset. *Scientific Data*, 10:1, 01 2023.
- [23] Byung-Hak Kim and Varun Ganapathi. Read, attend, and code: Pushing the limits of medical codes prediction from clinical notes by machines, 2021.
- [24] Tsung-Yi Lin, Priya Goyal, Ross Girshick, Kaiming He, and Piotr Dollár. Focal loss for dense object detection. In *2017 IEEE International Conference on Computer Vision (ICCV)*, pages 2999–3007, 2017.
- [25] Yang Liu, Hua Cheng, Russell Klopfer, Matthew R. Gormley, and Thomas Schaaf. Effective convolutional attention network for multi-label clinical document classification. In *Proceedings of the 2021 Conference on Empirical Methods in Natural Language Processing*, pages 5941–5953, Online and Punta Cana, Dominican Republic, November 2021. Association for Computational Linguistics.

- [26] Ilya Loshchilov and Frank Hutter. Decoupled weight decay regularization. In *7th International Conference on Learning Representations, ICLR 2019, New Orleans, LA, USA, May 6-9, 2019*. OpenReview.net, 2019.
- [27] Research ltd and Markets. AI in medical coding market size, share and trends analysis report by component (in-house, outsourced), by region (north america, europe, APAC, latin america, MEA), and segment forecasts, 2023 - 2030. <https://www.researchandmarkets.com/reports/5853844/>.
- [28] James Mullenbach, Sarah Wiegrefe, Jon Duke, Jimeng Sun, and Jacob Eisenstein. Explainable prediction of medical codes from clinical text. In *Proceedings of the 2018 Conference of the North American Chapter of the Association for Computational Linguistics: Human Language Technologies, Volume 1 (Long Papers)*, pages 1101–1111, New Orleans, Louisiana, June 2018. Association for Computational Linguistics.
- [29] Pandu Nayak. Understanding searches better than ever before. <https://blog.google/products/search/search-language-understanding-bert/>, Oct 2019.
- [30] U.S. National Library of Medicine. National center for biotechnology information. <https://pubmed.ncbi.nlm.nih.gov/>.
- [31] Mohit Pandey, Michael Fernandez, Francesco Gentile, Olexandr Isayev, Alexander Tropsha, Abraham Stern, and Artem Cherkasov. The transformational role of gpu computing and deep learning in drug discovery. *Nature Machine Intelligence*, 4:211–221, 03 2022.
- [32] Google SearchLiaison [@searchliaison]. BERT, our new way for google search to better understand language, is now rolling out to over 70 languages worldwide. [Tweet]. <https://twitter.com/dasaptaerwin/status/465577518565580801>, Feb 2023.
- [33] Zeyu Teng, Peng Cao, Min Huang, Zheming Gao, and Xingwei Wang. Multi-label borderline oversampling technique. *Pattern Recognition*, 145:109953, 2024.
- [34] Ashish Vaswani, Noam Shazeer, Niki Parmar, Jakob Uszkoreit, Llion Jones, Aidan N Gomez, Łukasz Kaiser, and Illia Polosukhin. Attention is all you need. In I. Guyon, U. Von Luxburg, S. Bengio, H. Wallach, R. Fergus, S. Vishwanathan, and R. Garnett, editors, *Advances in Neural Information Processing Systems*, volume 30. Curran Associates, Inc., 2017.
- [35] Thanh Vu, Dat Quoc Nguyen, and Anthony Nguyen. A label attention model for ICD coding from clinical text. In *Proceedings of the Twenty-Ninth International Joint Conference on Artificial Intelligence*. International Joint Conferences on Artificial Intelligence Organization, jul 2020.
- [36] Ben Wang and Aran Komatsuzaki. GPT-J-6B: A 6 Billion Parameter Autoregressive Language Model. <https://github.com/kingoflolz/mesh-transformer-jax>, May 2021.
- [37] Guangyu Wang, Xiaohong Liu, Zhen Ying, Guoxing Yang, Zhiwei Chen, Zhiwen Liu, Min Zhang, Hongmei Yan, Yuxing Lu, Yuanxu Gao, Kanmin Xue, Xiaoying Li, and Ying Chen. Optimized glycemetic control of type 2 diabetes with reinforcement learning: a proof-of-concept trial. *Nature Medicine*, 09 2023.
- [38] Zhichao Yang, Shufan Wang, Bhanu Pratap Singh Rawat, Avijit Mitra, and Hong Yu. Knowledge injected prompt based fine-tuning for multi-label few-shot icd coding, 2022.
- [39] Shurui Zhang, Bozheng Zhang, Fuxin Zhang, Bo Sang, and Wanchun Yang. Automatic ICD coding exploiting discourse structure and reconciled code embeddings. In *Proceedings of the 29th International Conference on Computational Linguistics*, pages 2883–2891, 2022.